Journal of Zhejiang University-SCIENCE B (Biomedicine & Biotechnology) 2024 25(6):513-528
www.jzus.zju.edu.cn; www.springer.com/journal/11585
E-mail: jzus_b@zju.edu.cn

Research Article
https://doi.org/10.1631/jzus.B2300303

Heme oxygenase 1 linked to inactivation of subchondral osteoclasts in osteoarthritis

Miao CHU[1,2*], Guangdong CHEN[1*], Kai CHEN[1,3*], Pengfei ZHU[1], Zhen WANG[4], Zhonglai QIAN[1], Huaqiang TAO[1✉], Yaozeng XU[1], Dechun GENG[1✉]

[1]*Department of Orthopedics, the First Affiliated Hospital of Soochow University, Suzhou 215006, China*
[2]*Department of Orthopedics, Yixing People's Hospital, Yixing 214200, China*
[3]*Department of Orthopedics, Hai'an People's Hospital, Hai'an 226600, China*
[4]*Department of Orthopedics, Suzhou Kowloon Hospital, Shanghai Jiao Tong University School of Medicine, Suzhou 215028, China*

Abstract: Osteoarthritis (OA) is a chronic progressive osteoarthropathy in the elderly. Osteoclast activation plays a crucial role in the occurrence of subchondral bone loss in early OA. However, the specific mechanism of osteoclast differentiation in OA remains unclear. In our study, gene expression profiles related to OA disease progression and osteoclast activation were screened from the Gene Expression Omnibus (GEO) repository. GEO2R and Funrich analysis tools were employed to find differentially expressed genes (DEGs). Gene Ontology (GO) and Kyoto Encyclopedia of Genes and Genomes (KEGG) enrichment analyses demonstrated that chemical carcinogenesis, reactive oxygen species (ROS), and response to oxidative stress were mainly involved in osteoclast differentiation in OA subchondral bone. Furthermore, fourteen DEGs that are associated with oxidative stress were identified. The first ranked differential gene, heme oxygenase 1 (*HMOX1*), was selected for further validation. Related results showed that osteoclast activation in the pathogenesis of OA subchondral bone is accompanied by the downregulation of *HMOX1*. Carnosol was revealed to inhibit osteoclastogenesis by targeting *HMOX1* and upregulating the expression of antioxidant protein in vitro. Meanwhile, carnosol was found to alleviate the severity of OA by inhibiting the activation of subchondral osteoclasts in vivo. Our research indicated that the activation of osteoclasts due to subchondral bone redox dysplasia may serve as a significant pathway for the advancement of OA. Targeting *HMOX1* in subchondral osteoclasts may offer novel insights for the treatment of early OA.

Key words: Osteoclast; Oxidative stress; Osteoarthritis (OA); Heme oxygenase 1 (HMOX1); Carnosol

1 Introduction

Osteoarthritis (OA) is a chronic joint disease caused by fibrosis, chapping, and the loss of articular cartilage (Xia et al., 2014), which now affects 300 million people worldwide. Many clinical symptoms, such as joint pain, swelling, and stiffness, caused by OA seriously influence patients' quality of life and even lead to disability (Bijlsma et al., 2011; Martel-Pelletier et al., 2016; Abramoff and Caldera, 2020). Meanwhile, long-term OA is an important cause of cardiovascular events and other systemic diseases. With the rapidly aging society, the incidence of OA in the population presents a rapidly rising trend, which creates a heavy burden on families and society.

Osteoclasts are derived from mononuclear hematopoietic marrow lineage cells that fuse on the bone surface under the regulation of the receptor activator of the nuclear factor-κB (NF-κB) ligand (RANKL) (Cappariello et al., 2014; Drissi and Sanjay, 2016; Wang et al., 2020). Abnormal osteoclast action is often associated with bone destruction and immune response in arthritic bone disease. In early OA, the self-repair of articular cartilage increases the secretion of RANKL in osteocytes, which leads to the overproduction of osteoclasts in subchondral bone and increased bone

✉ Dechun GENG, szgengdc@suda.edu.cn
Huaqiang TAO, 20224032009@stu.suda.edu.cn
* The three authors contributed equally to this work
Miao CHU, https://orcid.org/0000-0002-1779-3866
Dechun GENG, https://orcid.org/0000-0003-4375-2803
Huaqiang TAO, https://orcid.org/0000-0002-3601-0089

Received May 8, 2023; Revision accepted Aug. 9, 2023; Crosschecked June 7, 2024

resorption (Agidigbi and Kim, 2019; Tateiwa et al., 2019; Su et al., 2022). As a result, subchondral bone thickness was reduced and the remodeling rate was increased. Some scholars have also suggested that osteoclast hyperactivation may be a crucial source of pain in OA (Zhu et al., 2019). Meanwhile, osteoclasts and chondrocytes interact during the development of OA, triggering the progression of OA.

Oxidative stress is a phenomenon caused by the imbalance between metabolites such as reactive oxygen species (ROS) and the corresponding antioxidant defense system, leading to a disruption of cellular damage (Zorov et al., 2014; Kimball et al., 2021). At physiological concentrations, ROS participate in multiple metabolic pathways to protect cells from oxidative damage (Zhu et al., 2022). In the joints of patients with OA, the inflammatory response and microenvironment changes can lead to microenvironment hypoxia, while a hypoxic environment can promote immune disorder and secrete a large number of inflammatory factors, ROS, and matrix metalloproteinases (MMPs), ultimately leading to oxidative damage and an inflammatory response (Apel and Hirt, 2004; Wang et al., 2022); therefore, regulating oxidative stress is considered a potential scheme in the occurrence of OA. Numerous studies have revealed that ROS-activated cascade signals participate in osteoclast differentiation and lifespan (Boyce, 2013; Andreev et al., 2020). However, the underlying oxidative stress mechanisms of osteoclast activation in OA remain unclear. In this study, we integrated an analysis of relevant biomarkers or molecular signal networks that represent potential cellular mechanisms in OA.

To shed light on the function of oxidative stress in osteoclast differentiation in early OA subchondral bone, a bioinformatics approach was chosen to predict the enrichment network and molecular interaction network. In addition, upstream microRNAs (miRNAs) of key differentially expressed genes (DEGs) were identified. The first ranked differential gene, heme oxygenase 1 (*HMOX1*), was then validated by a mouse model of OA. In our study, we investigated the impact of *HMOX1* regulation on subchondral bone osteoclast activation in OA. These results may help with the development of a new therapeutic approach in the near future for treating OA.

2 Materials and methods

2.1 Access to Gene Expression Omnibus (GEO) datasets

Our team searched the National Center for Biotechnology Information (NCBI) GEO database (https://www.ncbi.nlm.nih.gov/geo) for microarray gene datasets with the keywords “osteoarthritis” and “osteoclast.” The screening criteria were as follows: (1) reliable source; (2) detailed information with published papers; and (3) biological tissues from *Mus musculus*. Two gene expression profiles, GSE41342 on the GPL1261 platform and GSE176265 on the GPL6887 platform, were found for further analysis.

Series GSE41342 contains expression profiles of data from OA mice. Tissues were collected from the destabilization of the medial meniscus (DMM) model group and the sham operation group at 2, 4, 8, and 16 weeks after operation. The tissues were used for RNA isolation. The 4-week data of the two groups were selected for comparative analysis. Series GSE176265 contains expression profiles of data from bone marrow-derived macrophages (BMMs) upon RANKL treatment. We selected the 0 and 72 h data for comparative analysis. Please refer to the “Materials and methods” in supplementary information for detailed instructions on how to analyze or acquire target genes.

2.2 Cell culture and in vitro osteoclastogenesis assay

BMMs were extracted from the femurs and tibias of mice in the sham and OA groups, as reported previously (Yang et al., 2022). Cells were centrifuged and then cultured with minimum essential medium-α (MEM-α; Thermo Fisher Scientific, USA) containing 10% (volume fraction) fetal bovine serum (FBS; Thermo Fisher Scientific) and 30 ng/mL macrophage colony-stimulating factor (M-CSF; Yangming Biotechnology Co., Ltd., Hangzhou, China) in 100-mm dishes. The culture medium was changed once every two days. Subsequently, 30 ng/mL M-CSF and 50 ng/mL RANKL (Yangming Biotechnology Co., Ltd.) were added to the medium to induce osteoclast differentiation.

2.3 Western blot

BMMs obtained from mouse bone marrow were lysed in radio-immunoprecipitation assay (RIPA) buffer (Beyotime, Shanghai, China) for 20 min and centrifuged at 12 000*g* for 4 min. Then, we used a bicinchoninic

acid (BCA) assay kit (Beyotime) to determine the protein concentration. The primary antibodies of HMOX1 (ABclonal, Wuhan, China, A11919), acid phosphatase 5 (ACP5; ABclonal, A16338), cathepsin K (CTSK; ABclonal, A5871), matrix metallopeptidase 9 (MMP9; ABclonal, A0289), nuclear factor of activated T cells 2 (NFAT2; Abcam, Cambridge, UK, ab2796), nuclear factor erythroid 2-related factor 2 (Nrf2; Abcam, ab137550), Kelch-like ECH-associated protein 1 (Keap1; Abcam, ab227828), superoxide dismutase 2 (SOD2; Abcam, ab68155), and β-actin (ABclonal, AC006) were utilized. The membranes were incubated with primary antibodies and horseradish peroxidase-conjugated secondary antibodies. The relative gray level was detected using enhanced chemiluminescence (NCM Biotech, Suzhou, China). ImageJ (Bethesda, USA) was used to quantify protein expression.

2.4 Molecular docking

HMOX1 (PDB ID: 1N45) was downloaded from the Protein Data Bank (PDB) database (http://www.wwpdb.org). Then, the three-dimensional (3D) structure was downloaded from PubChem data (https://pubchem.ncbi.nlm.nih.gov) according to the small molecule, and the optimized small molecule was imported into AutoDockTools-1.5.6. POCASA 1.1 was used to predict protein binding sites. AutoDock Vina 1.1.2 and PyMOL 2.3.0 were utilized for docking and analysis.

2.5 Cell proliferation and viability assay

Carnosol (MedChemExpress, Shanghai, China) was dissolved in dimethyl sulfoxide (DMSO). We used a cell counting kit-8 (CCK-8) assay kit (Yeasen, Shanghai, China) to detect the cytotoxicity of carnosol for BMMs. Briefly, BMMs were plated in a 96-well plate (5×10^3 cells per well), treated with various concentrations of carnosol, and incubated for 72 h. The samples were incubated with MEM-α containing 10% (volume fraction) CCK-8 reagent for 3 h under strict protection from light. Finally, a microplate reader (BioTek, USA) was employed to detect the absorbance at 450 nm.

2.6 qRT-PCR

Cells from different groups were prepared for total RNA extraction using TRIzol Reagent (Beyotime). A NanoDrop 2000 spectrophotometer (Thermo Fisher Scientific) was employed to detect the concentration of RNA. Synthesized complementary DNA (cDNA) was designed as a template for real-time polymerase chain reaction (PCR). Subsequently, reverse transcription-quantitative PCR (RT-qPCR) was used to evaluate the different messenger RNA (mRNA) expression levels of *HMOX1*, *CTSK*, *MMP9*, *NFAT2*, *Nrf2*, NAD(P)H: quinone oxidoreductase 1 (*NQO1*), *SOD1*, *SOD2*, and catalase (*CAT*). LightCycler® 480 software (Roche Diagnostics International Ltd., Switzerland) was employed to measure the gene levels. The comparative $2^{-\Delta\Delta C_T}$ method was used to calculate fold change. Details about the forward and reverse primers of all target genes are listed in Table S1.

2.7 Tartrate-resistant acid phosphatase (TRAP) staining

BMMs were cultured with MEM-α containing RANKL, M-CSF, and a certain concentration of carnosol for 4 d. Samples were fixed with paraformaldehyde (Beyotime) for 15 min after osteoclast formation. After washing, the staining solution was prepared according to the instructions using the TRAP Kit (Yangming Biotechnology Co., Ltd.). After staining, osteoclast morphology was observed under the microscope (Axiovert 40C, Zeiss, Germany), and the number of osteoclasts in each group was counted by ImageJ.

2.8 Bone resorption assay

Osteoclastic function was detected using a bone resorption assay. BMMs were plated onto bovine bone slices (Yangming Biotechnology Co., Ltd.) after treatment with 50 ng/mL RANKL and 30 ng/mL M-CSF. Eight days later, an FEI Quanta 250 scanning electron microscope (Hillsboro, USA) was used to detect resorption pits on the bone slices. ImageJ was utilized to quantify the absorption area.

2.9 Cell immunofluorescence staining

BMMs were plated on coverslips at a density of 3×10^4 cells per well in MEM-α with different interventions. Subsequently, all cells were fixed with 4% (0.04 g/mL) paraformaldehyde, followed by infiltration with Triton X-100 (Beyotime) for 15 min. The primary antibody against HMOX1 (ABclonal, A1346) was added and incubated at 4 °C. Then, the secondary fluorescent antibody (Alexa Fluor® 488, Yeasen) and F-actin (Yeasen) were added for another 1 h. Images were obtained using a fluorescence microscope (Axio Imager 2, Zeiss).

2.10 ROS assay

An ROS assay kit (Beyotime) was employed in our study to detect ROS generation. Briefly, BMMs (3×10^4 cells per well) were plated and incubated with 50 ng/mL RANKL and 30 ng/mL M-CSF for 4 d after different interventions. After washing three times with serum-free MEM-α medium, samples were incubated with the fluorescent probe 2',7'-dichlorofluorescein diacetate (DCFH-DA) for 20 min at 37 ℃ under dark conditions. Subsequently, we used a Zeiss laser scanning confocal microscope (LSM510, Zeiss) to obtain pictures.

2.11 JC-1 staining

To evaluate the mitochondrial membrane potential of the cells, we conducted JC-1 staining. We cultured BMMs in 48-well plates with a cell density of 20 000 cells per well and induced their differentiation into osteoclasts in both the presence and absence of carnosol. Subsequently, we collected cell samples and washed them with phosphate-buffered solution (PBS). The cells were then incubated with JC-1 stain for 20 min at 37 ℃. Following incubation, the cells were again washed with PBS, and the nuclei were restained with 4',6-diamidino-2-phenylindole (DAPI). Fluorescent images were captured using a super-resolution confocal microscope (LSM510, Zeiss), and the fluorescence was quantified utilizing ImageJ.

2.12 MitoSOX red staining

MitoSOX red staining was employed to detect mitochondrial superoxide production. To interfere with osteoclast differentiation, we utilized the medium with or without carnosol. Cell samples were collected from each group and were incubated with MitoSOX red at 2 μmol/L for 30 min at 37 ℃. Following incubation and washing, nuclei were restained with DAPI, and a confocal microscope (LSM510, Zeiss) was used to capture fluorescent images.

2.13 Transmission electron microscopy (TEM)

BMMs were treated with 50 ng/mL RANKL, 30 ng/mL M-CSF, and carnosol. After suitable intervention treatments, the samples were fixed with 2.5% (volume fraction) glutaraldehyde and were then dehydrated in a series of ethanol solutions. Subsequently, the treated cells were sectioned and observed using a transmission electron microscope from Hitachi (Model H-7650, Japan).

2.14 DMM-induced OA mouse model

Twenty-one male C57BL/6 mice (eight weeks old) were used in our study. They were divided into three groups: the sham group (only incised the medial skin of the patella), the OA group (DMM), and the carnosol group (DMM+carnosol articular injection). For DMM surgery, the knee joint of each mouse was skinned and disinfected. After incision of the skin and joint capsule, the medial meniscus tibial ligament was severed, and the medial meniscus was dissociated to cause instability (Glasson et al., 2007). In the treatment group, a total of 200 μg/kg of carnosol per knee was administered via intra-articular injection for four weeks (once a week until execution).

2.15 Micro-computed tomography (CT) analysis

The right knees of each group of mice were collected, fixed in 10% (volume fraction) neutral formalin for 48 h, and scanned with a micro-CT scanner (SkyScan 1176, Belgium). The machine parameters were set to 9 μm resolution, 0.7° rotation angle, and 170 mA current. The obtained data were reconstructed in three dimensions using software such as Recon, Dataviewer, CTan, and Mimics (Materialise). Additionally, bone mineral density (BMD; g/cm^3) was quantified.

2.16 Histological analysis

Four weeks after dewaxing, knee samples were taken for fixation and decalcification. These samples were then dehydrated and sliced into 6-μm-thick sections. We then performed hematoxylin and eosin (H&E) staining and safranin O-fast green staining according to the previous methods (Hu et al., 2020; Tao et al., 2021). Subsequently, the slices were subjected to TRAP (Yangming Biotechnology Co., Ltd.) to observe osteoclasts. Immunohistochemistry (IHC) was used to detect oxidative stress-related genes in all groups. Briefly, these slices were incubated with primary antibodies against HMOX1 (ABclonal; A1346) and its corresponding secondary antibodies. The expression and localization of HMOX1 were analyzed. We used an Axiovert 40 C optical microscope (Zeiss) to obtain images. To investigate the expression of oxidative stress-related genes in osteoclasts of subchondral bone, we conducted tissue immunofluorescence co-staining with

the corresponding oxidative stress-related genes and osteoclast biomarker CTSK, following established protocols. The specific antibodies utilized in this study were SOD2 (ABclonal, A1340), Nrf2 (ABclonal, A21508), and NQO1 (ABclonal, A19586).

2.17 Statistical analysis

GraphPad Prism 8.0 software (Santiago, USA) was utilized for statistical processing. Data are shown as mean±standard errors of the mean (SEM). Student's *t*-test was used to compare the normal distribution between the data of the two groups. One-way analysis of variance (ANOVA) and Tukey's test were used to compare the data of multiple groups with a normal distribution. A *P*-value of less than 0.05 was treated as statistically significant.

3 Results

3.1 Oxidative stress was identified as the key signal in osteoclast differentiation in OA

The DEGs of two gene expression profiles (GSE41342 and GSE176265) were identified using GEO2R, the online data analysis tool (Loeser et al., 2013; Kim et al., 2021). The dataset obtained after analysis using GEO2R for two gene expression profiles (GSE41342 and GSE176265) was analyzed using volcano plots. DEGs and expression trends are shown in Fig. 1a. A total of 206 co-expressed differential genes were found based on $\log_2$(fold change) ($\log_2$FC) of ⩾0.5 and adjusted *P*-value of <0.05 (Fig. 1b). In Table S2, we provide a comprehensive list of the names of these 206 specific differential genes. The 148 DEGs were screened from upregulated genes of two gene expression profiles, and 58 DEGs were screened from downregulated genes. Then, we submitted 206 co-expressed differential genes to the Metascape website (https://metascape.org/gp/index.html#/main/step1) and selected the organism *M. musculus* for follow-up analysis. We uploaded all analysis results to the oebiotech website (https://cloud.oebiotech.cn). Gene Ontology (GO)/Kyoto Encyclopedia of Genes and Genomes (KEGG) bubble plots were obtained using OECloud tools. As shown in Figs. 1c and 1d, the top three enriched biological process (BP) terms were vasculature development, collagen metabolic progress, and response to wounding. The top three enriched cellular component (CC) terms were collagen-containing extracellular matrix, extracellular matrix, and external encapsulating structure. The top three enriched molecular function (MF) terms were collagen binding, growth factor binding, and extracellular matrix structural constituent. KEGG pathway enrichment analysis revealed that these genes were involved in many signaling pathways, including extracellular matrix (ECM)–receptor interaction, proteoglycans in cancer, and focal adhesion. We submitted 206 genes to the STRING database (https://string-db.org) and chose organisms for *M. musculus*. The Protein-Protein Interaction (PPI) network was analyzed and constructed (Fig. S1). Seven molecular complex detection (MCODE) components were constructed with the screened DEGs (Fig. S2).

We then acquired oxidative stress-related genes from the PathCards website (https://pathcards.genecards.org) and the KEGG Pathway database. A total of 684 oxidative stress-related genes were found (Table S3). We then intersected the 684 genes with the 206 genes we had previously obtained. Venn diagrams were produced using FunRich software (http://www.funrich.org), and a total of 14 intersective genes were found (Fig. 1e). We placed the analyzed PPI data into Cytoscape software (https://cytoscape.org) and the results were plotted into a network diagram (Fig. 1f). The descriptions and functions of the 14 intersecting genes were acquired from the GeneCards website (https://www.genecards.org) (Table S4). To explore the functions of these 14 intersective genes, GO annotation and KEGG pathway analyses were employed. PPI enrichment analysis and MCODE cluster analysis were used to identify interactive hub genes. According to Fig. 1g, our findings indicated that the pathways of chemical carcinogenesis-ROS-*M. musculus* and pathways in cancer-*M. musculus* were found to be significantly enriched. This was further illustrated by the results of the MCODE1 analyses (Fig. 1h). The interactions of DEGs were input into Cytoscape software to screen out the important and valuable key genes. The top four hub nodes were identified, which, in descending order, are *HMOX1*, insulin-like growth factor 1 (*IGF1*), fibronectin (*FN1*), and hypoxia-inducible factor 1-α (*HIF1A*). To identify upstream miRNAs, we used the miRWalk database (http://mirwalk.umm.uni-heidelberg.de) and constructed a miRNA-mRNA regulatory network. As a result, 828 miRNA-mRNA pairs were identified (Fig. 1i). Taken together, oxidative stress-related genes may play crucial roles in osteoclasts in the pathogenesis of OA.

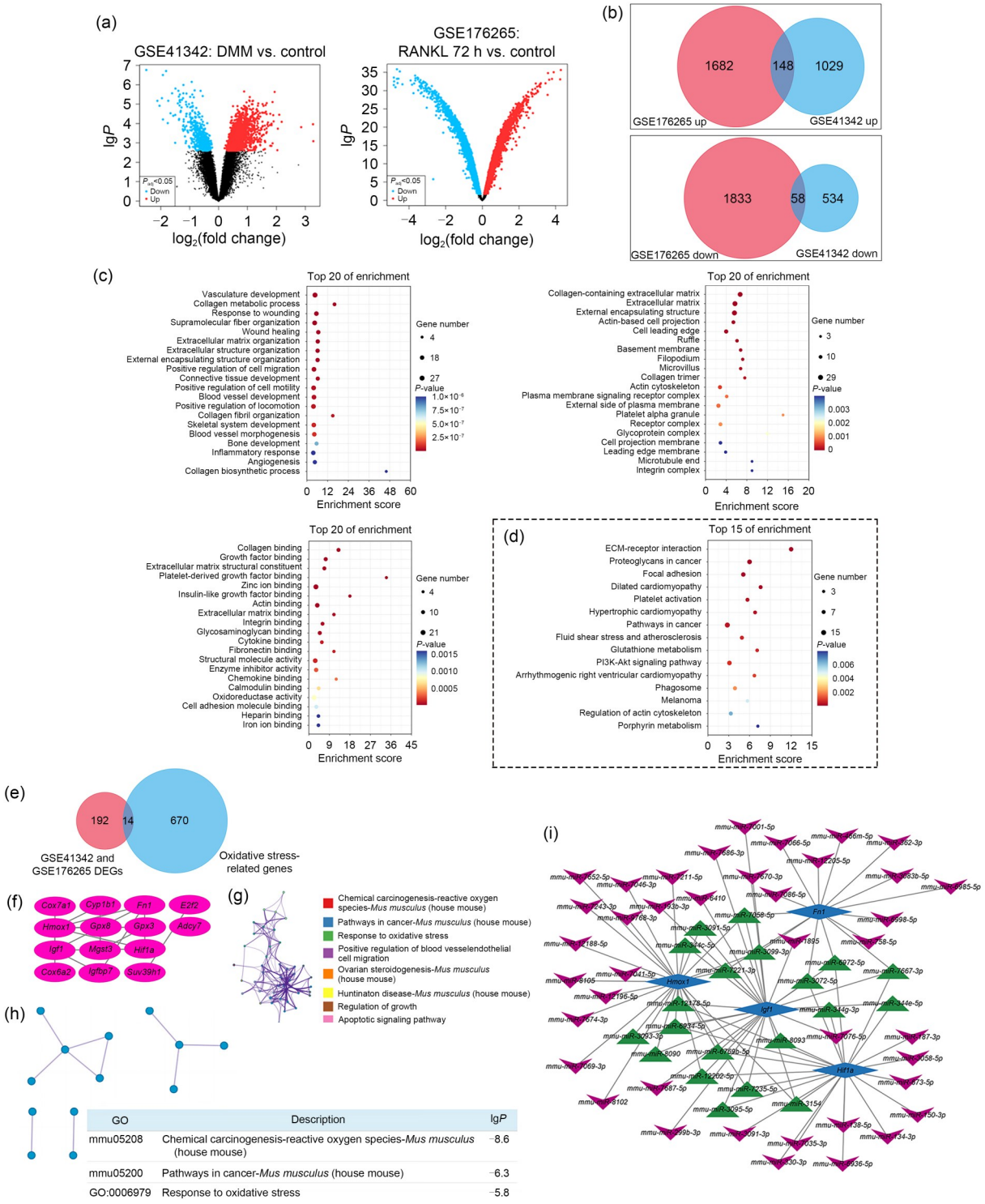

GO	Description	lg*P*
mmu05208	Chemical carcinogenesis-reactive oxygen species-*Mus musculus* (house mouse)	−8.6
mmu05200	Pathways in cancer-*Mus musculus* (house mouse)	−6.3
GO:0006979	Response to oxidative stress	−5.8

Fig. 1 Oxidative stress as the key signal in osteoclast differentiation in OA. (a) Volcano plots of the dataset obtained in GSE41342 and GSE176265. (b) Data intersection of DEGs. (c, d) Bubble plots of GO functional enrichment (c) and KEGG pathway enrichment (d) analysis results, including biological process, cellular component, molecular function, and enrichment KEGG pathways. (e) Fourteen co-expressed differentially genes were screened using a Venn diagram. (f) The intersecting genes were plotted into a network diagram. (g) Network of enriched 14 intersecting genes. (h) PPI network and MCODE components. (i) Prediction of miRNAs and construction of the miRNA-mRNA regulatory network. OA: osteoarthritis; DEGs: differentially expressed genes; GO: Gene Ontology; KEGG: Kyoto Encyclopedia of Genes and Genomes; PPI: Protein-Protein Interaction; MCODE: molecular complex detection; miRNA: microRNA; mRNA: messenger RNA; P_{adj}: adjusted *P*-value.

3.2 HMOX1 was involved in osteoclast differentiation in OA

Based on previous bioinformatics screening, we identified that HMOX1 may play an important role in osteoclast differentiation in OA. We extracted bone marrow cells from the sham group mice and the OA group mice to induce osteoclasts. Western blot and RT-qPCR results showed that the expression of HMOX1 was downregulated in the OA group (Figs. 2a and 2b).

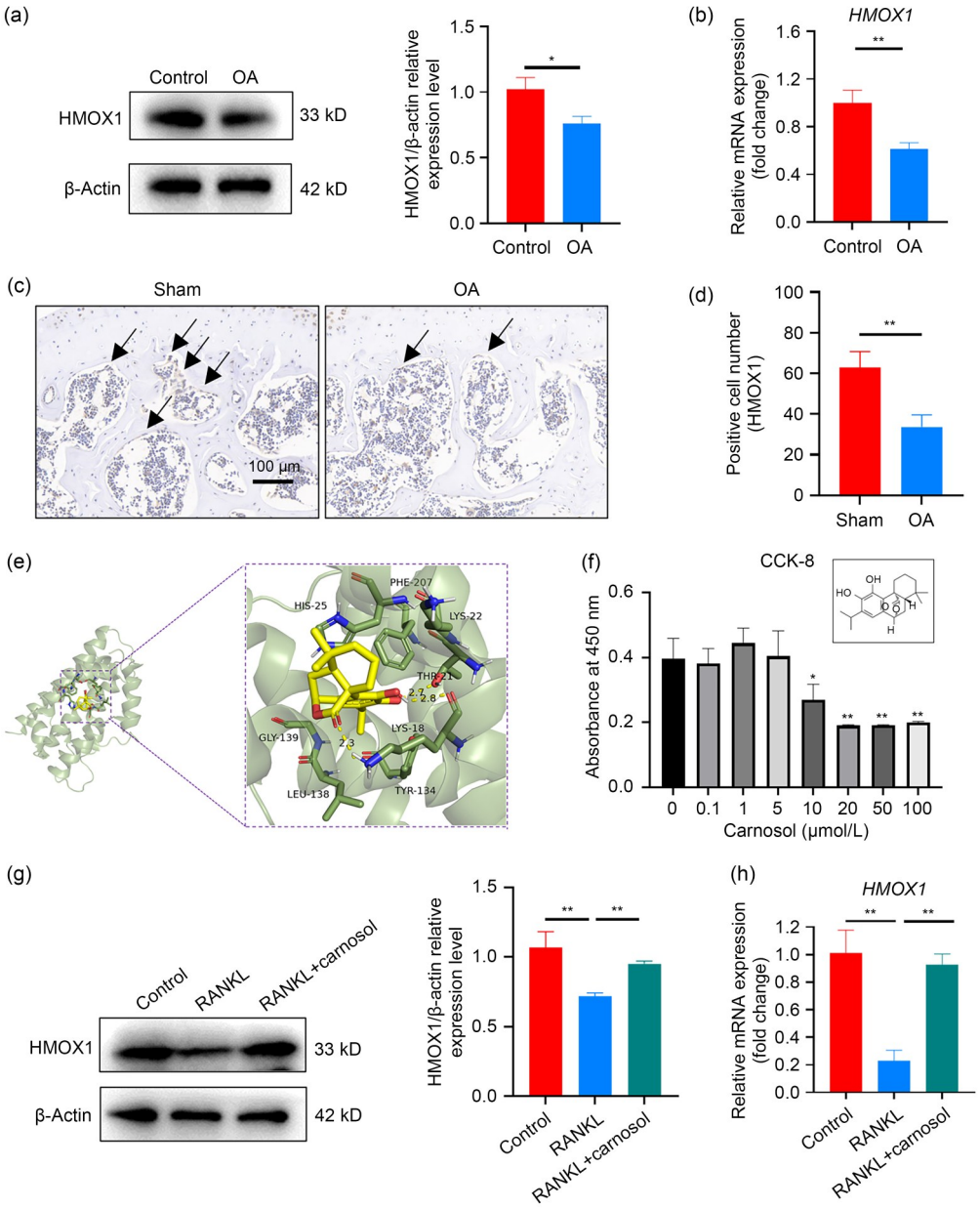

Fig. 2 HMOX1 involved in osteoclast differentiation in OA. (a) Western blot and quantitative analysis of HMOX1 in BMM-induced osteoclasts between the sham group and OA group mice. (b) RT-qPCR analysis of the mRNA expression levels of *HMOX1*. (c, d) Immunohistochemical staining and quantitative analysis for HMOX1 of decalcified bone sections, with black arrows pointing to HMOX1$^+$ cells. (e) Molecular docking. (f) CCK-8 assay of carnosol, n=5. $^*P$<0.05 and $^{**}P$<0.01, vs. 0 μmol/L carnosol. (g) Western blot and quantitative analysis of HMOX1 after treatment with carnosol. (h) RT-qPCR analysis of the mRNA expression levels of *HMOX1* after treatment with carnosol. Data are expressed as mean±standard errors of the mean (SEM), n=3. $^*P$<0.05, $^{**}P$<0.01. HMOX1: heme oxygenase 1; OA: osteoarthritis; BMMs: bone marrow-derived macrophage; RT-qPCR: reverse transcription-quantitative polymerase chain reaction; mRNA: messenger RNA; CCK-8: cell counting kit-8; RANKL: receptor activator of nuclear factor-κB (NF-κB) ligand.

Immunohistochemical staining also indicated that the expression of HMOX1 in the subchondral bone of the OA group was decreased (Figs. 2c and 2d).

We screened carnosol, an important monomer that targets HMOX1, for follow-up experiments. Molecular docking results showed that the binding energy of carnosol and HMOX1 was 30.1 kJ/mol, which proved that carnosol had a good binding effect with HMOX1. Carnosol interacts with HMOX1 mainly through hydrogen bond formation and hydrophobic forces (Fig. 2e). Furthermore, CCK-8 results revealed that treatment with carnosol at concentrations under 5 μmol/L had no toxicity to BMMs (Fig. 2f). We then used 5 μmol/L carnosol to intervene RANKL-induced osteoclast differentiation. Western blot and RT-PCR results showed that carnosol treatment significantly promoted the expression of HMOX1 (Figs. 2g and 2h).

3.3 Carnosol inhibited osteoclastogenesis and bone resorption in vitro

First, we used 50 ng/mL RANKL and 30 ng/mL M-CSF to induce osteoclast differentiation. Then, 5 μmol/L carnosol was added to intervene in this process. Western blot results revealed that carnosol inhibited the expression of osteoclast-related proteins, including ACP5, CTSK, MMP9, and NFAT2 (Fig. 3a). Subsequently, RT-qPCR results indicated that carnosol inhibited the gene expression of *CTSK*, *MMP9*, *NFAT2*, and *ACP5* as well (Fig. 3b). After 4 d of treatment, the TRAP staining results revealed that the $TRAP^+$ osteoclasts in the carnosol treatment group prominently decreased compared with those in the RANKL group (Figs. 3c and 3d). Furthermore, the bone resorption assay showed that carnosol inhibited osteoclastic resorption (Figs. 3e and 3f). Taken together, our data indicated that carnosol effectively regulates RANKL-induced osteoclast formation.

3.4 Carnosol inhibited osteoclastogenesis by regulating oxidative stress signaling in mitochondria-dependent pathways

We previously demonstrated the significant osteoclast inhibitory effect of carnosol. Considering that carnosol can target HMOX1 signaling, we then detected the expression of HMOX1 in cells after carnosol intervention. Immunofluorescence staining showed that HMOX1 expression was downregulated after RANKL intervention. When treated with carnosol, osteoclast differentiation was inhibited and intracellular HMOX1 expression was increased (Figs. 4a and 4c). ROS are important mediators in the redox reaction in vivo, and the expression levels of cellular ROS were detected under this intervention. Our fluorescence results indicated that carnosol treatment significantly inhibited ROS production (Figs. 4b and 4d). Subsequently, we detected the expression level of intracellular antioxidant proteins after carnosol intervention. Our western blot results indicated that carnosol promoted the expression of Nrf2 and SOD2, and downregulated Keap1 (Fig. 4e). RT-qPCR analysis suggested that carnosol promoted the expression of *Nrf2*, *NQO1*, *SOD1*, *SOD2*, and *CAT*, which are all important signaling molecules mediating antioxidant defense (Fig. 4f).

Previously, our study identified that carnosol inhibits osteoclast differentiation by suppressing ROS production. Considering that the main source of ROS is the substrate end of the respiratory chain in the inner mitochondrial membrane, we further explored the effect of carnosol on BMM mitochondrial function. Our results demonstrated that, during osteoclast differentiation, the mitochondrial membrane potential was increased, which was significantly reduced after treatment with carnosol (Figs. 5a and 5c). MitoSOX staining demonstrated a noteworthy elevation in intracellular mitochondrial superoxide expression during osteoclast differentiation. However, the formation of mitochondrial superoxide was significantly suppressed upon intervention with carnosol (Figs. 5b and 5d). Further, we examined the mitochondrial morphology of each group of cells using TEM following the intervention. Our findings revealed that, upon RANKL intervention, there was a noticeable increase in the number of mitochondria and lysosomes within the cells, accompanied by a blurred appearance of the mitochondrial cristae. However, these effects were effectively mitigated following carnosol intervention (Fig. 5e). Taken together, these results suggested that carnosol may regulate the level of cellular oxidative stress through the mitochondrial pathway.

3.5 Carnosol inhibited subchondral osteoclast differentiation and delayed the progression of OA in vivo

Previous studies have shown that changes in the microstructure and mechanical properties of subchondral bone are related to the onset and progression

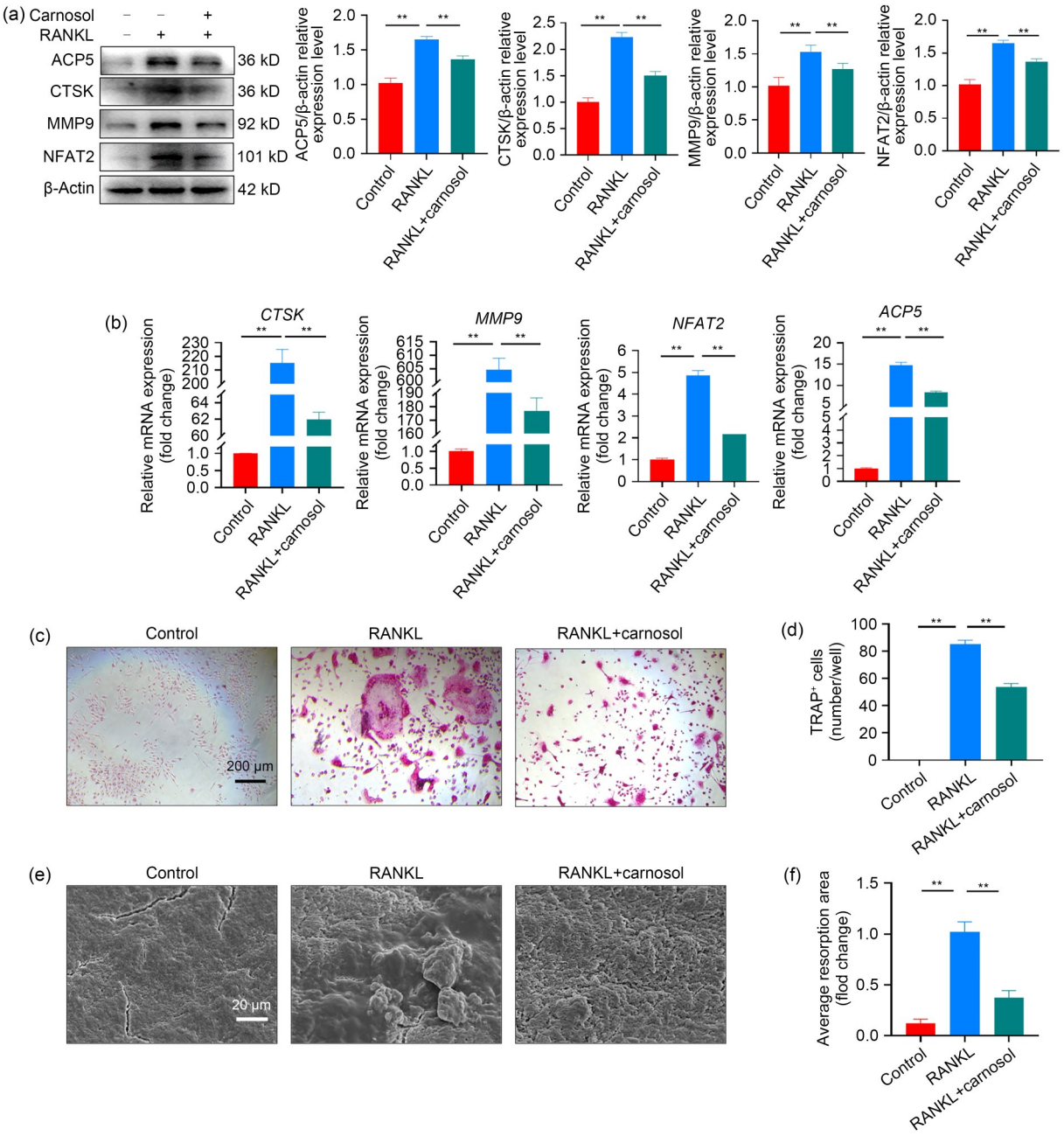

Fig. 3 Effects of carnosol on osteoclastogenesis and bone resorption. (a) The protein levels and quantitative analysis of ACP5, CTSK, MMP9, and NFAT2 after carnosol treatment. (b) RT-qPCR analysis of the mRNA expression levels of *CTSK*, *MMP9*, *NFAT2*, and *ACP5*. (c, d) Representative TRAP staining images and quantification of TRAP$^+$ cells. (e, f) Scanning electron microscopy images of the bone resorption area after carnosol treatment. Data are expressed as mean±standard errors of the mean (SEM), n=3. $^{**}P$<0.01. ACP5: acid phosphatase 5; CTSK: cathepsin K; MMP9: matrix metallopeptidase 9; NFAT2: nuclear factor of activated T cells 2; RT-qPCR: reverse transcription-quantitative polymerase chain reaction; mRNA: messenger RNA; TRAP: tartrate-resistant acid phosphatase; RANKL: receptor activator of nuclear factor-κB (NF-κB) ligand.

of OA. The activation of subchondral osteoclasts is an important factor leading to subchondral bone disorders. In vivo, carnosol was injected into the articular cavity in OA mice at a dose of 200 μg/kg once a week. Micro-CT results implied that carnosol delayed the progression of OA (Fig. 6a). Fig. 6b demonstrated a two-dimensional scanned image of subchondral bone. Subchondral bone thickness analysis revealed that the subchondral bone in the group of mice with OA was observed to be thin. However, following carnosol

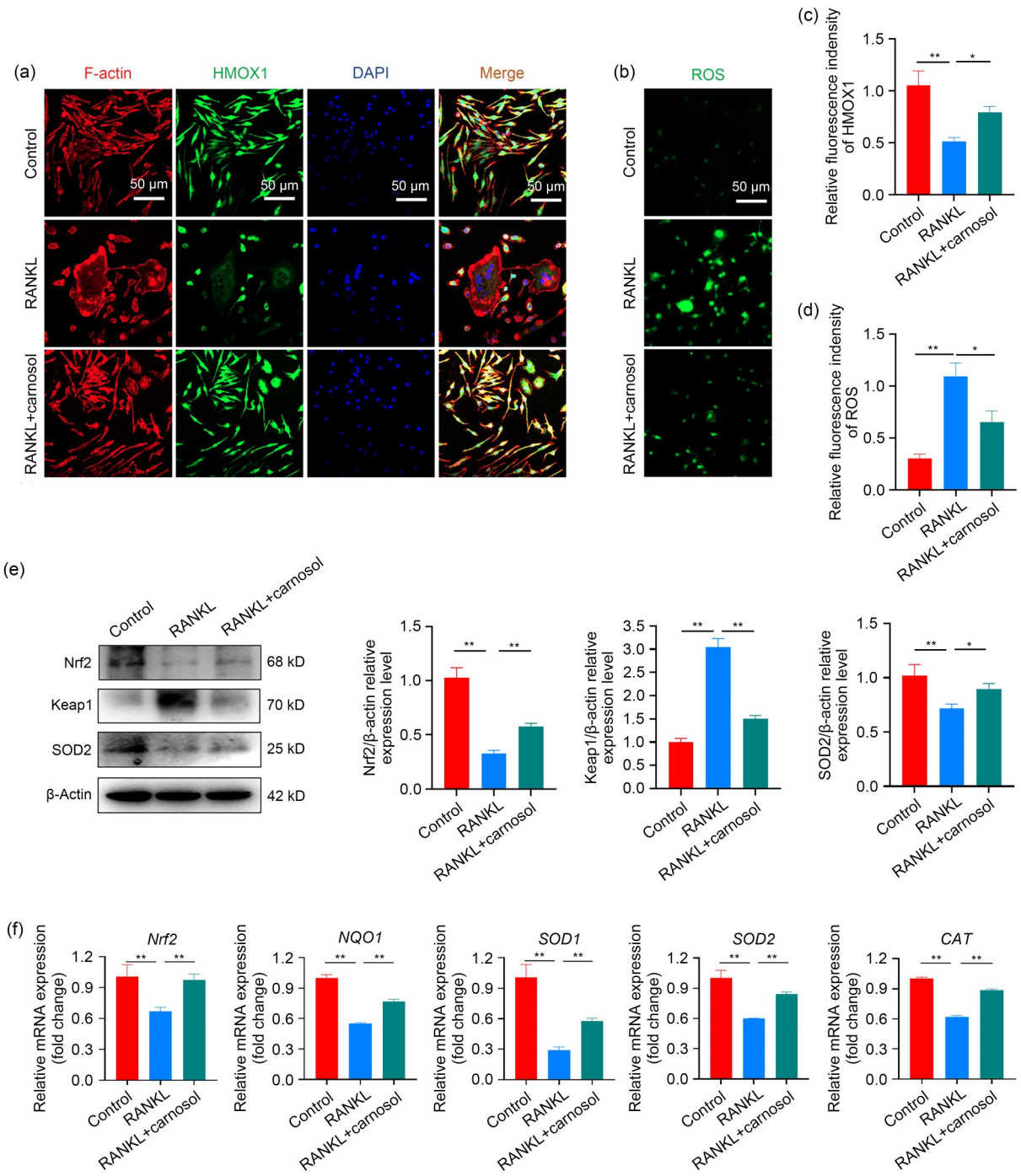

Fig. 4 Inhibitive role of carnosol in osteoclastogenesis by regulating oxidative stress signaling. (a) Representative images of immunofluorescence staining: red (F-actin), green (HMOX1), and blue (nuclei). (b) Representative images of RANKL-induced ROS generation in the BMMs after treatment with carnosol. (c) Quantitative analysis of HMOX1. (d) Quantitative analysis of ROS staining. (e) Western blot results and quantitative analyses of Nrf2, Keap1, and SOD2 proteins after carnosol treatment. (f) RT-qPCR analyses of the mRNA expression levels of *Nrf2*, *NQO1*, *SOD1*, *SOD2*, and *CAT*. Data are expressed as mean±standard errors of the mean (SEM), n=3. $^{*}P$<0.05, $^{**}P$<0.01. HMOX1: heme oxygenase 1; RANKL: receptor activator of nuclear factor-κB (NF-κB) ligand; ROS: reactive oxygen species; BMMs: bone marrow-derived macrophages; Nrf2: nuclear factor erythroid 2-related factor 2; Keap1: Kelch-like ECH-associated protein 1; SOD: superoxide dismutase; RT-qPCR: reverse transcription-quantitative polymerase chain reaction; mRNA: messenger RNA; NQO1: NAD(P)H:quinone oxidoreductase 1; CAT: catalase; DAPI: 4',6-diamidino-2-phenylindole.

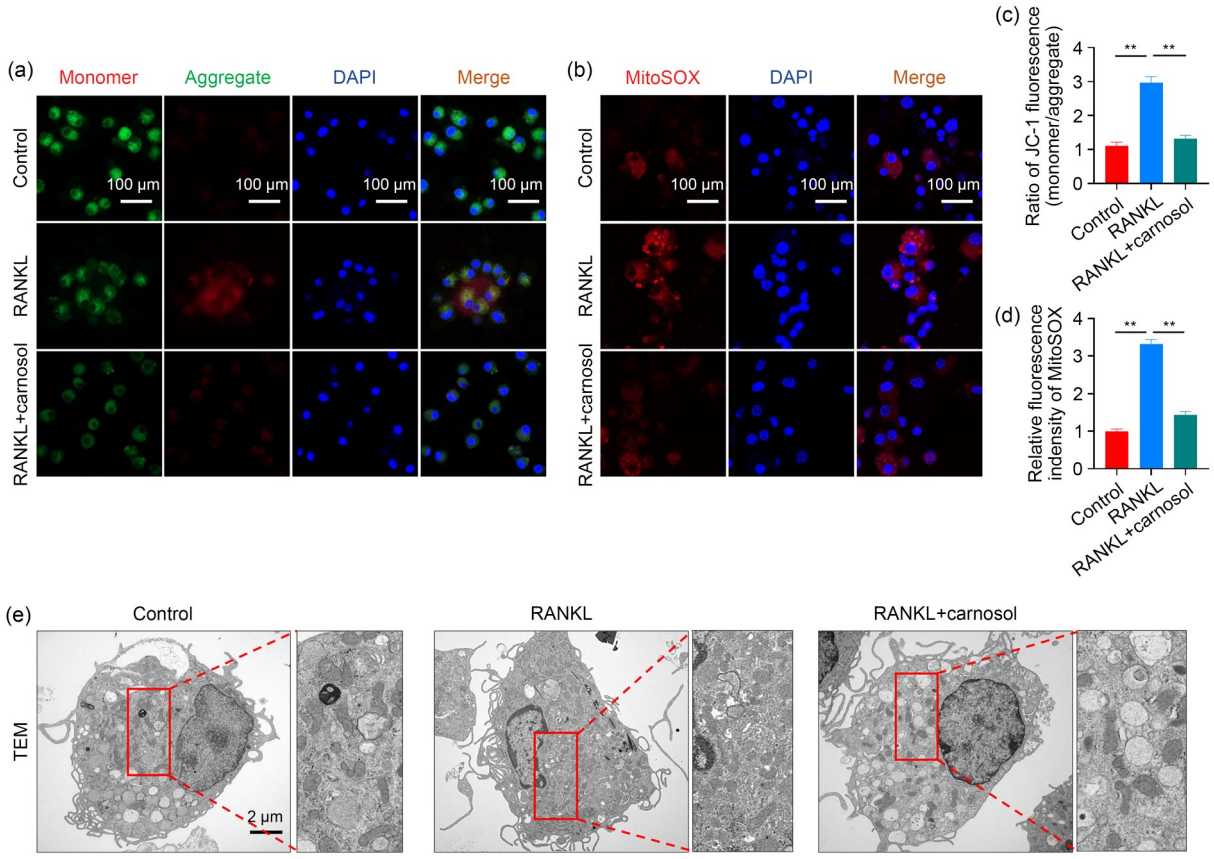

Fig. 5 Inhibitive role of carnosol in osteoclastogenesis by regulating mitochondrial function. (a, c) JC-1 staining for mitochondrial membrane potential measurement and quantitative analysis of monomer/aggregate. (b, d) Immunofluorescence staining and quantitative analysis of MitoSOX. (e) Electron microscopic structure of each group. Data are expressed as mean±standard errors of the mean (SEM), n=3. $^{**}P$<0.01. DAPI: 4',6-diamidino-2-phenylindole; RANKL: receptor activator of nuclear factor-κB (NF-κB) ligand; TEM: transmission electron microscopy.

intervention, there was a significant reversal in the thickness of the subchondral bone. A quantitative analysis showed that the subchondral BMD in the carnosol intervention group was higher than that in the OA group, which suggested that carnosol treatment has a positive regulatory effect on relieving OA subchondral bone disorders (Fig. 6c). Immunohistochemical staining revealed significantly higher expression of HMOX1 in the subchondral bone of OA mice after carnosol intervention (Figs. 6d and 6e). Subsequently, H&E staining and safranin O-fast green staining were performed on the knee tissue of mice for the histological evaluation of cartilage tissue. As shown in Figs. 6f–6i, the surfaces of the joints of OA mice were rough and cell degeneration and arrangement were disordered. However, carnosol effectively improved that performance and alleviated the disorder of subchondral bone structure. Furthermore, TRAP staining suggested that carnosol inhibited subchondral osteoclastic activation in the OA group (Figs. 6j and 6k). Taken together, carnosol may have a positive therapeutic effect on OA by way of targeted inhibition of subchondral osteoclastic activation and improved subchondral bone microstructure.

Furthermore, we investigated the impact of carnosol intervention on the oxidative stress levels in osteoclasts of subchondral bone in OA mice. Immunofluorescence staining was used to examine the effects of carnosol. We utilized CTSK (green) to label osteoclasts and observed that the expression of SOD2, Nrf2, and NQO1, which are markers associated with oxidative stress, was reduced in the subchondral bone of mice with OA. However, when carnosol was administered via intra-articular injection, the expression of antioxidant markers in subchondral osteoclasts was effectively increased (Fig. 7). This ultimately led to the inhibition of subchondral osteoclast activation in OA.

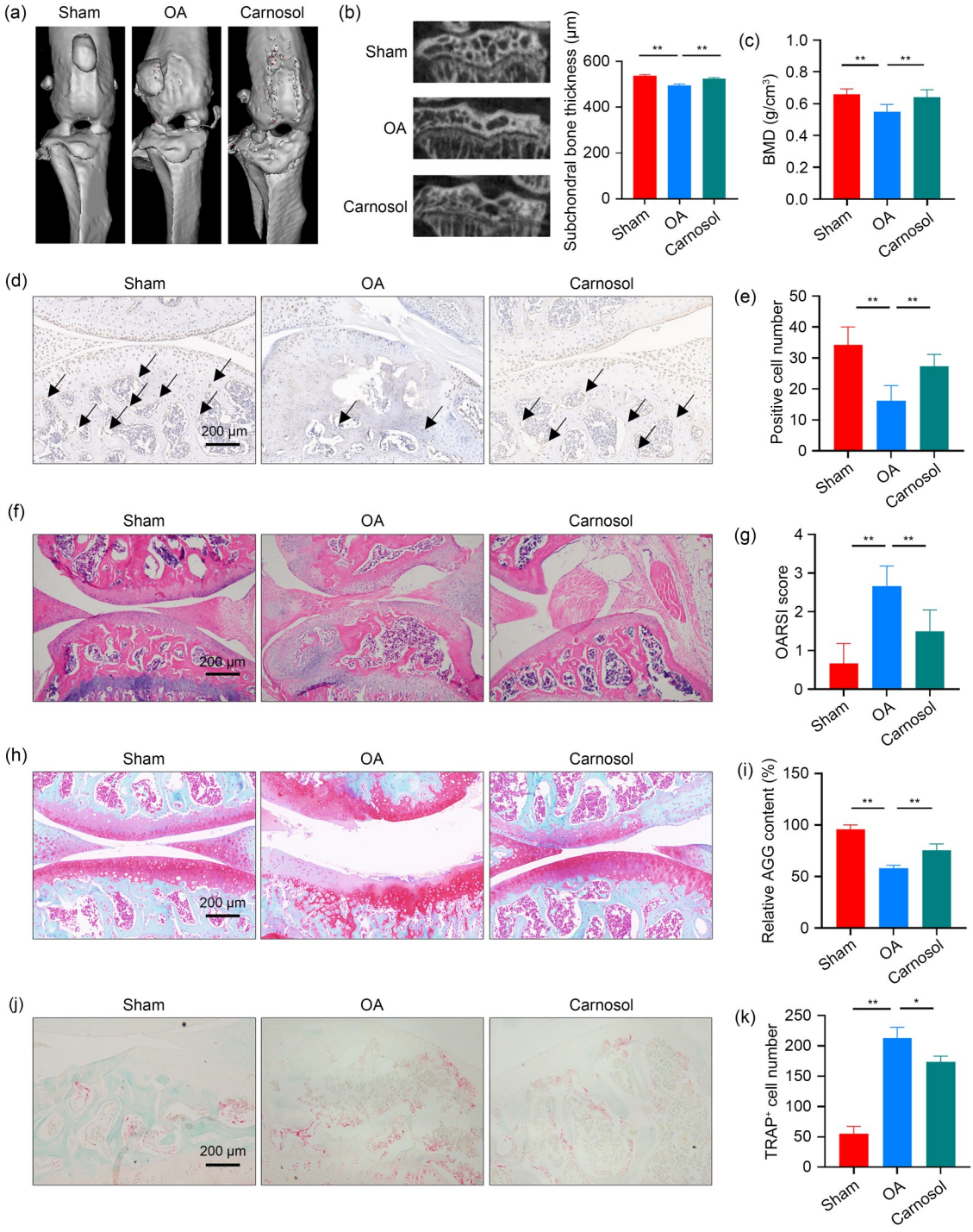

Fig. 6 Effects of carnosol on subchondral osteoclast differentiation and the progression of OA. (a) Representative micro-CT images of the mouse knee joint. (b) Two-dimensional (2D) scanned images of subchondral bone and subchondral bone thickness measurement. (c) Quantitative analysis of subchondral BMD. (d, e) Immunohistochemical staining and quantitative analysis for HMOX1 of decalcified bone sections, with black arrows pointing to HMOX1$^+$ cells. (f) H&E staining of the sections. (g) OARSI score. (h) Safranin O-fast green staining images of the sections. (i) Relative glycosaminoglycan aggrecan (AGG) content. (j) TRAP staining of the sections. (k) Quantitative analysis of TRAP$^+$ osteoclasts. Data are expressed as mean±standard errors of the mean (SEM), n=7. $^*P$<0.05, $^{**}P$<0.01. OA: osteoarthritis; CT: computed tomography; HMOX1: heme oxygenase 1; H&E: hematoxylin and eosin; OARSI: Osteoarthritis Research Society International; TRAP: tartrate-resistant acid phosphatase; BMD: bone mineral density.

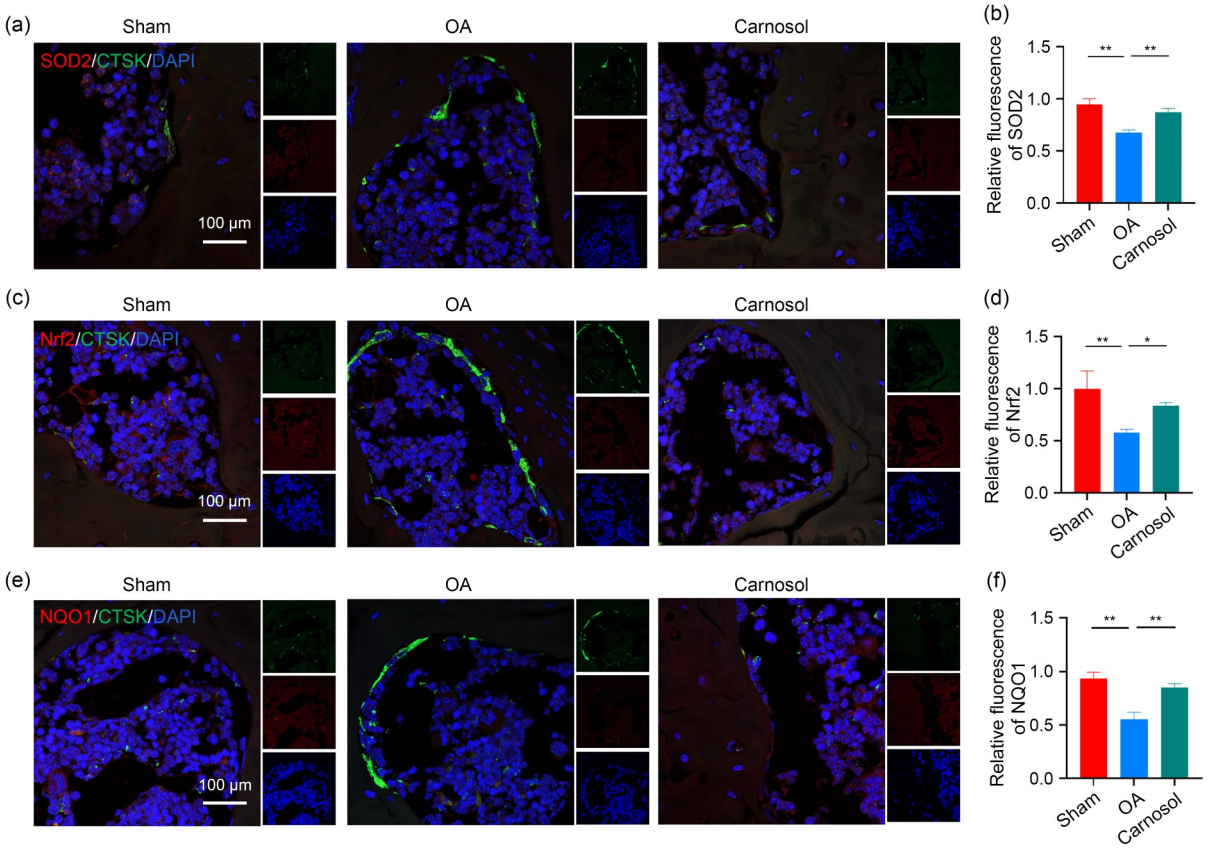

Fig. 7 Effects of carnosol on the expression of antioxidant markers in subchondral osteoclasts in vivo. (a, b) Immunofluorescence staining and quantitative analysis of SOD2 and CTSK in OA subchondral bone. (c, d) Immunofluorescence staining and quantitative analysis of Nrf2 and CTSK in OA subchondral bone. (e, f) Immunofluorescence staining and quantitative analysis of NQO1 and CTSK in OA subchondral bone. Data are expressed as mean±standard errors of the mean (SEM), n=7. $^{*}P$<0.05, $^{**}P$<0.01. SOD2: superoxide dismutase 2; CTSK: cathepsin K; OA: osteoarthritis; Nrf2: nuclear factor erythroid 2-related factor 2; NQO1: NAD(P)H:quinone oxidoreductase 1; DAPI: 4',6-diamidino-2-phenylindole.

4 Discussion

OA is a common chronic joint disease in the clinic. Its pathological features mainly include articular cartilage injury, abnormal remodeling of subchondral bone, and synovial inflammation (Glyn-Jones et al., 2015). Articular cartilage and subchondral bone constitute a functional complex unit and influence each other in the course of OA (Li et al., 2013). Recent research has found that abnormal remodeling of subchondral bone participates in the onset of OA and may even be the initiating factor of OA (Cui et al., 2016; Hu et al., 2021; Li et al., 2021). Abnormalities in subchondral bone remodeling in the early stages of OA mainly manifest as increased bone resorption, which leads to decreased subchondral bone mass and changes in bone microstructure.

Osteoclasts are special end-differentiated cells originating from the mononuclear macrophage system (Pereira et al., 2018). Changes in osteoclast activity lead to bone resorption, which occurs in many bone and joint diseases. Overactivation of osteoclasts disrupts bone turnover and mediates related diseases such as peri-prosthesis osteolysis, osteoporosis, and OA (Boyle et al., 2003). Numerous studies have shown that osteoclasts initiate bone matrix degradation by secreting protons and lysosomal proteases (TRAP, MMP9, and CTSK) in the early stage of OA, thus leading to increased absorption of subchondral bone (Karsdal et al., 2014; Zhu et al., 2021). Abnormal mechanical stress load can also cause excessive activation of osteoclasts in OA subchondral bone.

Oxidative stress is regarded as an important risk factor for primary and secondary OA (Almeida and

Porter, 2019; Shen et al., 2021). Studies have shown that aging, mechanical stress, and inflammation increase the level of oxidative stress in the joints during the progression of OA (Lepetsos et al., 2019). Furthermore, oxidative stress leads to chondrocyte death, cell senescence, and increased expression of inflammatory cytokines (Shi et al., 2022). Recent studies have found that increased levels of oxidative stress lead to osteoclast activation, which promotes the onset of OA (Guo et al., 2022). However, research on the role of osteoclasts in oxidative stress during the onset of early OA is limited. The study of the regulatory network of oxidative stress in osteoclasts might provide new ideas to elucidate the specific mechanisms of OA. Bioinformatics analysis and experimentally validated approaches may open the door for OA disease research that can tap into biomarkers and related pathways.

In our study, two series, GSE176265 and GSE41342, were screened using the GEO database, and potential oxidative stress-related genes in osteoclasts in OA were analyzed using bioinformatics methods. After a series of analyses, we identified 14 DEGs related to oxidative stress in OA osteoclasts. The first four hub genes were *HMOX1*, *IGF1*, *FN1*, and *HIF1A*. Among them, HMOX1 is a rate-limiting enzyme in heme catabolism and is one of the most important antioxidant protection enzymes involved in inflammatory stimulation and biological oxidation reactions (Liu et al., 2018; Schipper et al., 2019). Previous studies have revealed that HMOX1 acts in osteoclast activation. Sakamoto et al. (2012) reported that deltamethrin suppressed osteoclastogenesis by upregulating HMOX1 signals. Yamaguchi et al. (2014) showed that tert-butylhydroquinone inhibited BMM-induced osteoclast differentiation by inducing HMOX1. These studies suggested that HMOX1 may be essential for maintaining bone mass balance in the body.

Our results showed that HMOX1 expression was downregulated in the knee subchondral bone of OA mice. In addition, the expression of HMOX1 in osteoclasts induced by BMMs from OA mice was decreased. Recognizing the significant benefits of traditional Chinese medicine in disease treatment, we then sought out suitable drug molecules that could target the activation of HMOX1. Through molecular docking, we successfully identified carnosol as a potential drug molecule. Furthermore, our experiments have confirmed that carnosol promotes the expression of HMOX1 in the differentiation of osteoclasts. The previous study conducted by Chen et al. (2020) has reported that carnosol is utilized for the treatment of lipopolysaccharide (LPS)-induced bone destruction, which is achieved by blocking RANKL-induced osteoclastogenesis through the regulation of the NF-κB and c-Jun N-terminal kinase (JNK) signaling pathways. Cai et al. (2022) reported that carnosol effectively reduced bone loss in ovariectomized mice by blocking RANKL-induced osteoclastogenesis through inhibiting the NF-κB pathway. In our study, we conducted further research to examine the specific effects of carnosol on osteoclastic activation. Additionally, we explored the impact of administering carnosol to the articular cavity on osteoclastic activation of subchondral bone and the progression of OA in mice.

In vitro results showed that carnosol significantly inhibited osteoclast activation and bone resorption. Mechanistically, carnosol inhibited ROS expression and upregulated antioxidant proteins during osteoclast differentiation in mitochondrial-dependent pathways. In vivo, carnosol inhibited the osteoclast formation of OA subchondral bone and effectively blocked the progression of OA. In recent years, the study of the function of subchondral bone in the progression of OA has received increasing attention. Few studies have focused on regulating oxidative stress levels in subchondral bone to retard the progression of OA. Studying the effects of oxidative stress in osteoclasts may provide another way to elucidate the mechanisms, and ultimately the treatment, of OA. In this research, these findings suggested that targeting the HMOX1 signaling cascade in subchondral osteoclasts may serve as a rational new therapeutic target against OA.

5 Conclusions

Subchondral osteoclastic activation plays a critical role in the progression of OA and has a significant impact on patient prognosis. Our study found that HMOX1, a key target in regulating the oxidative stress signaling cascade, has positive implications for regulating subchondral osteoclastic activation. We observed that carnosol inhibited BMM-induced osteoclastic activation by targeting HMOX1 signaling and upregulating the antioxidant system. In vivo, carnosol was found to alleviate OA progression by inhibiting subchondral

bone osteoclast activation; hence, targeting HMOX1 in subchondral osteoclasts may offer novel insights for the treatment of early OA.

Data availability statement

The datasets generated and/or analyzed during the current study are not publicly available but are available from the corresponding author on reasonable request.

Acknowledgments

This work was supported by the National Natural Science Foundation of China (Nos. 82272157, 82072425, and 82072498), the Natural Science Foundation of Jiangsu Province (No. BE2021650), the Priority Academic Program Development (PAPD) of Jiangsu Higher Education Institutions, the Program of Suzhou Health Commission (Nos. GSWS2022002 and GSWS2020121), the Jiangsu Medical Research Project (No. ZD2022014), the National and Local Engineering Laboratory of New Functional Polymer Materials (No. SDGC2205), and the Special Project of Diagnosis and Treatment Technology for Key Clinical Diseases in Suzhou (No. LCZX202003), China.

Author contributions

Miao CHU, Guangdong CHEN, and Huaqiang TAO designed the research strategy and worked with the animal models. Kai CHEN and Zhonglai QIAN performed immunohistochemical staining. Miao CHU, Guangdong CHEN, and Pengfei ZHU performed the in vitro assays. Zhen WANG, Yaozeng XU, and Dechun GENG performed the statistical analysis and wrote the manuscript. Huaqiang TAO and Dechun GENG revised the paper. All authors have read and approved the final manuscript, and therefore, have full access to all the data in the study and take responsibility for the integrity and security of the data.

Compliance with ethics guidelines

Miao CHU, Guangdong CHEN, Kai CHEN, Pengfei ZHU, Zhen WANG, Zhonglai QIAN, Huaqiang TAO, Yaozeng XU, and Dechun GENG declare that they have no conflict of interest.

All institutional and national guidelines for the care and use of laboratory animals were followed. All animal experiments and tests were guided and approved by the Animal Ethics Committee of the Soochow University (No. SUDA20221009A05).

References

Abramoff B, Caldera FE, 2020. Osteoarthritis: pathology, diagnosis, and treatment options. *Med Clin North Am*, 104(2): 293-311. https://doi.org/10.1016/j.mcna.2019.10.007

Agidigbi TS, Kim C, 2019. Reactive oxygen species in osteoclast differentiation and possible pharmaceutical targets of ROS-mediated osteoclast diseases. *Int J Mol Sci*, 20(14): 3576. https://doi.org/10.3390/ijms20143576

Almeida M, Porter RM, 2019. Sirtuins and FoxOs in osteoporosis and osteoarthritis. *Bone*, 121:284-292. https://doi.org/10.1016/j.bone.2019.01.018

Andreev D, Liu MD, Weidner D, et al., 2020. Osteocyte necrosis triggers osteoclast-mediated bone loss through macrophage-inducible C-type lectin. *J Clin Invest*, 130(9):4811-4830. https://doi.org/10.1172/jci134214

Apel K, Hirt H, 2004. Reactive oxygen species: metabolism, oxidative stress, and signal transduction. *Annu Rev Plant Biol*, 55:373-399. https://doi.org/10.1146/annurev.arplant.55.031903.141701

Bijlsma JW, Berenbaum F, Lafeber FP, 2011. Osteoarthritis: an update with relevance for clinical practice. *Lancet*, 377(9783):2115-2126. https://doi.org/10.1016/s0140-6736(11)60243-2

Boyce BF, 2013. Advances in the regulation of osteoclasts and osteoclast functions. *J Dent Res*, 92(10):860-867. https://doi.org/10.1177/0022034513500306

Boyle WJ, Simonet WS, Lacey DL, 2003. Osteoclast differentiation and activation. *Nature*, 423(6937):337-342. https://doi.org/10.1038/nature01658

Cai P, Yan SC, Lu Y, et al., 2022. Carnosol inhibits osteoclastogenesis *in vivo* and *in vitro* by blocking the RANKL-induced NF-κB signaling pathway. *Mol Med Rep*, 26:225. https://doi.org/10.3892/mmr.2022.12741

Cappariello A, Maurizi A, Veeriah V, et al., 2014. The great beauty of the osteoclast. *Arch Biochem Biophys*, 558:70-78. https://doi.org/10.1016/j.abb.2014.06.017

Chen YZ, Lu JW, Li SH, et al., 2020. Carnosol attenuates RANKL-induced osteoclastogenesis in vitro and LPS-induced bone loss. *Int Immunopharmacol*, 89:106978. https://doi.org/10.1016/j.intimp.2020.106978

Cui Z, Crane J, Xie H, et al., 2016. Halofuginone attenuates osteoarthritis by inhibition of TGF-β activity and H-type vessel formation in subchondral bone. *Ann Rheum Dis*, 75(9):1714-1721. https://doi.org/10.1136/annrheumdis-2015-207923

Drissi H, Sanjay A, 2016. The multifaceted osteoclast; far and beyond bone resorption. *J Cell Biochem*, 117(8):1753-1756. https://doi.org/10.1002/jcb.25560

Glasson SS, Blanchet TJ, Morris EA, 2007. The surgical destabilization of the medial meniscus (DMM) model of osteoarthritis in the 129/SvEv mouse. *Osteoarthritis Cartilage*, 15(9):1061-1069. https://doi.org/10.1016/j.joca.2007.03.006

Glyn-Jones S, Palmer AJR, Agricola R, et al., 2015. Osteoarthritis. *Lancet*, 386(9991):376-387. https://doi.org/10.1016/s0140-6736(14)60802-3

Guo YN, Cui SJ, Tian YJ, et al., 2022. Chondrocyte apoptosis in temporomandibular joint osteoarthritis promotes bone resorption by enhancing chemotaxis of osteoclast precursors. *Osteoarthritis Cartilage*, 30(8):1140-1153. https://doi.org/10.1016/j.joca.2022.04.002

Hu SL, Zhang CW, Ni LB, et al., 2020. Stabilization of HIF-1α alleviates osteoarthritis via enhancing mitophagy. *Cell Death Dis*, 11(6):481. https://doi.org/10.1038/s41419-020-2680-0

Hu WH, Chen YQ, Dou C, et al., 2021. Microenvironment in

subchondral bone: predominant regulator for the treatment of osteoarthritis. *Ann Rheum Dis*, 80(4):413-422. https://doi.org/10.1136/annrheumdis-2020-218089

Karsdal MA, Bay-Jensen AC, Lories RJ, et al., 2014. The coupling of bone and cartilage turnover in osteoarthritis: opportunities for bone antiresorptives and anabolics as potential treatments? *Ann Rheum Dis*, 73(2):336-348. https://doi.org/10.1136/annrheumdis-2013-204111

Kim MJ, Kim HS, Lee S, et al., 2021. Hexosamine biosynthetic pathway-derived O-GlcNAcylation is critical for RANKL-mediated osteoclast differentiation. *Int J Mol Sci*, 22(16):8888. https://doi.org/10.3390/ijms22168888

Kimball JS, Johnson JP, Carlson DA, 2021. Oxidative stress and osteoporosis. *J Bone Jt Surg*, 103(15):1451-1461. https://doi.org/10.2106/jbjs.20.00989

Lepetsos P, Papavassiliou KA, Papavassiliou AG, 2019. Redox and NF-κB signaling in osteoarthritis. *Free Radical Biol Med*, 132:90-100. https://doi.org/10.1016/j.freeradbiomed.2018.09.025

Li B, Chen KZ, Qian ND, et al., 2021. Baicalein alleviates osteoarthritis by protecting subchondral bone, inhibiting angiogenesis and synovial proliferation. *J Cell Mol Med*, 25(11): 5283-5294. https://doi.org/10.1111/jcmm.16538

Li GY, Yin JM, Gao JJ, et al., 2013. Subchondral bone in osteoarthritis: insight into risk factors and microstructural changes. *Arthritis Res Ther*, 15(6):223. https://doi.org/10.1186/ar4405

Liu XH, Ji CX, Xu L, et al., 2018. Hmox1 promotes osteogenic differentiation at the expense of reduced adipogenic differentiation induced by BMP9 in C3H10T1/2 cells. *J Cell Biochem*, 119(7):5503-5516. https://doi.org/10.1002/jcb.26714

Loeser RF, Olex AL, McNulty MA, et al., 2013. Disease progression and phasic changes in gene expression in a mouse model of osteoarthritis. *PLoS ONE*, 8:e54633. https://doi.org/10.1371/journal.pone.0054633

Martel-Pelletier J, Barr AJ, Cicuttini FM, et al., 2016. Osteoarthritis. *Nat Rev Dis Primers*, 2:16072. https://doi.org/10.1038/nrdp.2016.72

Pereira M, Petretto E, Gordon S, et al., 2018. Common signalling pathways in macrophage and osteoclast multinucleation. *J Cell Sci*, 131(11):jcs216267. https://doi.org/10.1242/jcs.216267

Sakamoto H, Sakai E, Fumimoto R, et al., 2012. Deltamethrin inhibits osteoclast differentiation via regulation of heme oxygenase-1 and NFATc1. *Toxicol Vitro*, 26(6):817-822. https://doi.org/10.1016/j.tiv.2012.05.005

Schipper HM, Song W, Tavitian A, et al., 2019. The sinister face of heme oxygenase-1 in brain aging and disease. *Prog Neurobiol*, 172:40-70. https://doi.org/10.1016/j.pneurobio.2018.06.008

Shen C, Gao M, Chen HM, et al., 2021. Reactive oxygen species (ROS)-responsive nanoprobe for bioimaging and targeting therapy of osteoarthritis. *J Nanobiotechnol*, 19:395. https://doi.org/10.1186/s12951-021-01136-4

Shi YF, Chen JX, Li SL, et al., 2022. Tangeretin suppresses osteoarthritis progression via the Nrf2/NF-κB and MAPK/NF-κB signaling pathways. *Phytomedicine*, 98:153928. https://doi.org/10.1016/j.phymed.2022.153928

Su WP, Liu GQ, Mohajer B, et al., 2022. Senescent preosteoclast secretome promotes metabolic syndrome associated osteoarthritis through cyclooxygenase 2. *eLife*, 11:e79773. https://doi.org/10.7554/eLife.79773

Tao HQ, Li WM, Zhang W, et al., 2021. Urolithin A suppresses RANKL-induced osteoclastogenesis and postmenopausal osteoporosis by, suppresses inflammation and downstream NF-κB activated pyroptosis pathways. *Pharmacol Res*, 174: 105967. https://doi.org/10.1016/j.phrs.2021.105967

Tateiwa D, Yoshikawa H, Kaito T, 2019. Cartilage and bone destruction in arthritis: pathogenesis and treatment strategy: a literature review. *Cells*, 8(8):818. https://doi.org/10.3390/cells8080818

Wang G, Wang YN, Yang QZ, et al., 2022. Metformin prevents methylglyoxal-induced apoptosis by suppressing oxidative stress in vitro and in vivo. *Cell Death Dis*, 13:29. https://doi.org/10.1038/s41419-021-04478-x

Wang XY, Yamauchi K, Mitsunaga T, 2020. A review on osteoclast diseases and osteoclastogenesis inhibitors recently developed from natural resources. *Fitoterapia*, 142:104482. https://doi.org/10.1016/j.fitote.2020.104482

Xia BJ, Chen D, Zhang JS, et al., 2014. Osteoarthritis pathogenesis: a review of molecular mechanisms. *Calcif Tissue Int*, 95(6):495-505. https://doi.org/10.1007/s00223-014-9917-9

Yamaguchi Y, Sakai E, Sakamoto H, et al., 2014. Inhibitory effects of tert-butylhydroquinone on osteoclast differentiation via up-regulation of heme oxygenase-1 and down-regulation of HMGB1 release and NFATc1 expression. *J Appl Toxicol*, 34(1):49-56. https://doi.org/10.1002/jat.2827

Yang C, Tao HQ, Zhang HF, et al., 2022. TET2 regulates osteoclastogenesis by modulating autophagy in OVX-induced bone loss. *Autophagy*, 18(12):2817-2829. https://doi.org/10.1080/15548627.2022.2048432

Zhu CY, Shen SW, Zhang SH, et al., 2022. Autophagy in bone remodeling: a regulator of oxidative stress. *Front Endocrinol*, 13:898634. https://doi.org/10.3389/fendo.2022.898634

Zhu SA, Zhu JX, Zhen GH, et al., 2019. Subchondral bone osteoclasts induce sensory innervation and osteoarthritis pain. *J Clin Invest*, 129(3):1076-1093. https://doi.org/10.1172/jci121561

Zhu XB, Chan YT, Yung PSH, et al., 2021. Subchondral bone remodeling: a therapeutic target for osteoarthritis. *Front Cell Dev Biol*, 8:607764. https://doi.org/10.3389/fcell.2020.607764

Zorov DB, Juhaszova M, Sollott SJ, 2014. Mitochondrial reactive oxygen species (ROS) and ROS-induced ROS release. *Physiol Rev*, 94(3):909-950. https://doi.org/10.1152/physrev.00026.2013

Supplementary information

Materials and methods; Tables S1–S4; Figs. S1 and S2